Available online at www.sciencedirect.com
SCIENCE DIRECT®
International Journal of Solids and Structures 42 (2005) 287–305
INTERNATIONAL JOURNAL OF SOLIDS and STRUCTURES
www.elsevier.com/locate/ijsolstr

The effect of interfacial properties on the cohesion of highly filled composite materials

F.H. Heukamp [a], E. Lemarchand [a,b,*], F.J. Ulm [a,*]

[a] *Department of Civil and Environmental Engineering, Massachusetts Institute of Technology, 77 Massachusetts Avenue, Cambridge, MA 02139, USA*
[b] *Laboratoire de Mécanique de Lille, UMR CNRS 8107, Boulevard Paul Langevin, 59655 Villeneuve d'Ascq, France*

Received 27 September 2002; received in revised form 8 July 2004
Available online 16 September 2004

Abstract

It has long been recognized that the cohesion of composite materials, in low confinement, is strongly affected by the properties of the interfacial transition zone (ITZ) between inclusions and matrix. While the effect of the ITZ on the elasticity properties of composites has been studied by many authors in the context of linear homogenization methods, the upscaling of the cohesion strength of highly filled composite materials has not been addressed. This is the focus of the non-linear homogenization procedure developed in this paper, which is based on the separation of the heterogeneous material system in phases of constant strength properties, a non-linear elastic representation of the limit stress state in each phase, and the definition of appropriate effective strain quantities that capture the morphological features of the microstructure. Applied to a three phase composite model composed of rigid inclusion, interface zone and matrix, the model provides a quantitative means of studying the effect of the interface cohesion and the interface volume fraction on the composite cohesion. In particular, we identify a critical interface-to-matrix cohesion ratio, below which the composite cohesion is smaller than the one of the matrix. Furthermore, the model lends itself readily to the study of the degradation of the interfacial properties in composite materials. This is shown for non-degraded and chemically softened cement-based materials, for which we provide conclusive evidence (1) that the interface strength properties of mortar are far more affected by chemical degradation than the one of the cement paste matrix; and (2) that chemical

* Corresponding authors. Address: Laboratoire de Mécanique de Lille, UMR CNRS 8107, Boulevard Paul Langevin, 59655 Villeneuve d'Ascq, France. Tel.: +1 617 253 3544; fax: +1 617 253 6044 (F.J. Ulm), tel.: +33 3 20 33 71 67; fax: +33 3 20 33 71 57 (E. Lemarchand).
E-mail addresses: eric.lemarchand@univ-lille1.fr (E. Lemarchand), ulm@mit.edu (F.J. Ulm).
URLs: http://www.univ-lille1.fr/lml (E. Lemarchand), http://cist.mit.edu (F.J. Ulm).

0020-7683/$ - see front matter
doi:10.1016/j.ijsolstr.2004.07.007

degradation does affect the mechanical strength performance of the cement paste not only through a change of volume proportions (i.e. increase of porosity), but as well through a pure chemical softening of the solid's cohesion.

Keywords: Micromechanics; Composite materials; Interfacial transition zone; Cohesion; Secant methods; Chemical softening

1. Introduction

It is common practice, in mechanics of materials, to characterize the low confinement tensile–compressive strength domain of isotropic composite materials by means of two material properties: the friction coefficient δ and the cohesion c. These material properties are conveniently determined from the uniaxial compressive strength f_c' and the uniaxial tensile strength f_t' of the material, and the use of a cohesive-frictional strength criterion. For instance, using a Drucker–Prager criterion, δ and c are obtained by means of interpolation of the two uniaxial strength values in the $\sqrt{J_2} \times \Sigma_M$ stress invariant halfplane ($J_2 = \frac{1}{2}\mathrm{tr}(\underline{\underline{S}} \cdot \underline{\underline{S}}) =$ 2nd invariant of the deviator stress, $\underline{\underline{S}} = \underline{\underline{\Sigma}} - \Sigma_M \underline{\underline{\delta}}$, $\Sigma_M = \frac{1}{3}\mathrm{tr}\,\underline{\underline{\Sigma}} =$ mean stress; $\underline{\underline{\delta}} =$ Kronecker Delta) from:

$$F(\underline{\underline{\Sigma}}) = \sqrt{J_2} + \delta\Sigma_M - c \leqslant 0 \tag{1}$$

$$0 \leqslant c = \frac{2}{\sqrt{3}} \frac{f_c' f_t'}{f_c' + f_t'} \leqslant \frac{2}{\sqrt{3}} f_t'; \quad 0 \leqslant \delta = \sqrt{3}\frac{f_c' - f_t'}{f_c' + f_t'} \leqslant \sqrt{3} \tag{2}$$

An open question is how the macroscopic material properties of the composite material relate to the properties of its microscopic constituents, that is matrix, inclusions and interfaces. For purpose of illustration, Table 1 summarizes some results of a recent test campaign on cement-based composite materials. The materials used in this test campaign are a cement paste, i.e. the matrix of cement-based composites, and a mortar prepared at a water-cement ratio $w/c = 0.5$, using a Type I Portland cement. The mortar contains narrowly graded Nevada sand with $d_{60} = 0.23$ mm and $d_{30} = 0.17$ mm ($d_\alpha = \beta$ mm means that α,% of the sand grains have a diameter less than β mm) at a water-cement-sand ratio of $w/c/s = 1/2/4$. This corresponds to a sand volume fraction of roughly $f_I = 0.5$. A part of the material specimens were chemically softened by means of calcium leaching in a highly concentrated ammonium nitrate solution, generating a new material, described in details in Heukamp et al. (2001a,b). The leaching process leads to a dissolution of Portlandite minerals $Ca(OH)_2$ that account for about 20% of the solid volume of a cement paste. In addition, the Calcium-Silicate-Hydrates are partially decalcified. As equilibrium is reached, a strong increase in porosity has taken

Table 1
Measured tensile and compressive strength of a cement paste and a mortar, together with determined Drucker–Prager strength parameters, friction coefficient δ and cohesion c, and macroporosity

	Paste (matrix)		Mortar (composite)	
	Initial	Degraded	Initial	Degraded
Tensile strength f_t' [MPa]	1.87	0.87	3.48	0.94
Compressive strength f_c' [MPa]	54.1	3.2	36.6	3.0
Friction coefficient δ [1]	1.62	0.99	1.43	0.91
Cohesion c [MPa]	2.09	0.79	3.67	0.83
Macroporosity [1/100]	1.0	21.0	1.5	10.5

Note that the macroporosity is not the total porosity of the material but the porosity considered as a phase of the matrix in the sense of continuum micromechanics. This corresponds to the micrometer-range porosity of cement-based materials.

place, along with a substantial reduction in stiffness and strength of the remaining solid. It is interesting to note, from Table 1, the difference of the effect of inclusions on the tensile strength and the compressive strength. For the intact material, rigid sand inclusions clearly enhance the matrix tensile strength ($f'_t = 1.87 \rightarrow 3.48$ MPa), while they substantially reduce the compressive strength ($f'_c = 54.1 \rightarrow 36.6$ MPa). Similar trends are found for the chemically softened material, albeit less pronounced ($f'_t = 0.87 \rightarrow 0.94$ MPa; $f'_c = 3.2 \rightarrow 3.0$ MPa). While the composite strength enhancement in tension can be explained by crack arresting and crack kinking at inclusions of the governing fracture process in the matrix, that ultimately translate into a higher tensile strength of the composite (mortar) than the pure matrix strength (cement paste), the lower compressive strength of the composite implies that there are other mechanisms and material constituents at work. It has long been argued, for cement-based materials, that this particular behavior in low confinement was due to the "Interfacial Transition Zone" (ITZ), that is the interface between inclusion and matrix. Fig. 1 displays a typical SEM micrograph of the ITZ of a calcium depleted mortar, showing clearly the changing properties of the material in the ITZ away from the inclusion(aggregate). In general, this zone is characterized by an increased porosity and a different material composition (higher concentration of $Ca(OH)_2$, and non-hydrated cement particles) compared with the remaining matrix, reducing generally the composite compressive strength.

Fig. 2 displays the results in the $\sqrt{J_2} \times \Sigma_M$ stress invariant halfplane, from which the Drucker–Prager strength parameters, δ and c, are extracted. In low confinement that characterizes the tensile–compressive strength capacity, the different effect of inclusion on the tensile vs. compressive strength translates into a reduction of the friction coefficient δ and an increase of the composite cohesion c_{hom} (see Table 1). By contrast, in high confinement, the trends are inverted: the presence of inclusions leads to a frictional enhancement due to an increased local confinement, hence de-activating the ITZ. This phenomenon has been studied in details for cement-based materials both experimentally (Ulm et al., 2002; Heukamp et al., 2001b) and theoretically (Lemarchand et al., 2002); but goes beyond the scope of this paper that focusses on the low-confinement strength domain of highly filled composite materials, in which the interfacial properties significantly affect the cohesion.

More precisely, due to material processing, an interface zone around the inclusion almost invariably exists that can have different properties than the matrix material. The size of this zone can vary; but it is usually on the order of the characteristic microstructural size of the matrix material. The effects of the

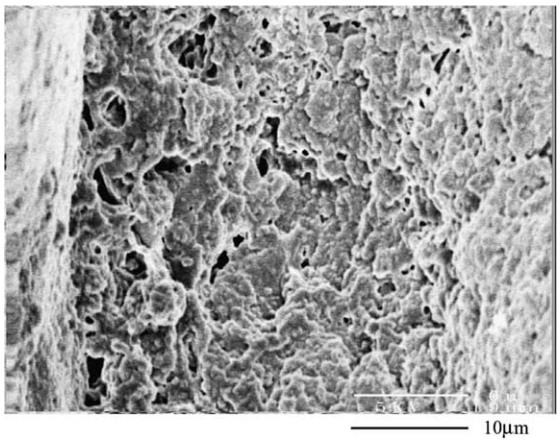

Fig. 1. SEM micrograph of the interfacial transition zone (ITZ) of a calcium depleted mortar, with sand inclusion (left) and matrix (right).

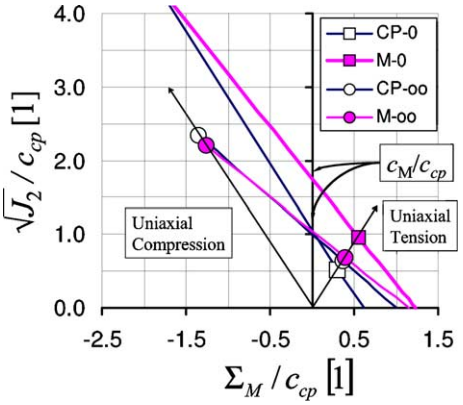

Fig. 2. Low confinement strength domain in the $\sqrt{J_2} \times \Sigma_M$-halfplane (normalized by the cement paste cohesion): CP-0 = undegraded cement paste (matrix); M-0 = undegraded mortar (composite); CP-oo=degraded cement paste; M-oo = degraded mortar.

ITZ on the elastic properties of composite materials have been addressed by many authors. For cement-based composites (Ramesh et al., 1996; Lutz and Zimmerman, 1996; Lutz et al., 1997; Li et al., 1999) and more recently Hashin and Monteiro (2002) proposed different linear upscaling schemes to calculate analytically the composite elastic properties and to determine the ITZ properties by inverse analysis. Garboczi and Berryman (2001) employed numerical techniques to predict the composite elastic properties for random microstructures with interfaces. However, the effect of the ITZ on the strength properties of the composite is harder to determine. One reason is that the mechanical properties of the ITZ are difficult to assess experimentally. The rare microhardness measurements reported by different authors show values between 25% and 40% of the bulk paste but vary strongly in the absolute values (Mehta and Monteiro, 1988; Yuji, 1988), and do not provide conclusive evidence of the governing parameters of the interface that ultimately affect the macroscopic strength. The aim of this paper is to quantify the effects of interfacial properties on the macroscopic cohesion of highly filled composite materials. This will be achieved by means of a non-linear micromechanics approach, which follows the one originally proposed by Ponte Castaneda (1991) and by Suquet (1997), and which has already been employed for the study of the frictional enhancement of highly filled composite materials in high confinement (Lemarchand et al., 2002). While developed around the topic of cement-based composites, the approach is sufficiently general to be extended to other particle composite materials, for which similar behavior have been found: filled epoxy resin (Ishai and Bodner, 1970), cemented soils (Consoli and Prietto, 1998; Ismael and Mollah, 1998), frozen sand (Re, 2000), metal-ceramic composites (Suresh and Mortensen, 1998), etc.

2. Elements of non-linear continuum micromechanics

Cement-based materials are composite materials that are characterized by a heterogeneous microstructure at different length scales. These range from nanometer, the characteristic length scale of Calcium-Silicate-Hydrate sheets (C-S-H), to decimeters, the largest aggregate size in concretes. Continuum Micromechanics offers a framework to address the relation between multiscale material heterogeneity and macroscopic material behavior. The guiding-principle of continuum micromechanics is a separation of the heterogeneous material into phases with constant material properties, leading to an estimation of the combined properties. A micromechanical analysis can be divided into three steps (see e.g. Zaoui, 2002):

(1) *Representation*, which is the physical description of the considered material system. It includes the identification of the representative element volume (r.e.v) and the phases therein. It has to obey the separability-of-scale-condition, which requires that the characteristic length scale of the r.e.v., say l, must be much smaller than the characteristic scale of the considered macroscopic structure, L, and much greater than the scale of the heterogeneities, d. The representation includes the geometry and morphology of the phases and their material properties (i.e. elastic properties or strength properties).
(2) *Localization*, which provides the link between the macroscopic constant strain (or stress state), prescribed on the boundary ∂V of the r.e.v., and the strain (or stress) in each individual phase.
(3) *Homogenization*, which is based on an averaging process, leads to the macroscopic properties of the r.e.v. They are a function of the properties of the microscopic phases.

In the following, these three steps are applied to estimate the effect of the ITZ on the cohesion of highly filled composite materials.

2.1. Geometrical and mechanical representations

The composite material system we consider is a set of three layered inclusions embedded in an infinite medium with homogenized properties. The three inclusions are the rigid inclusion, the ITZ, and the matrix. Fig. 3 gives a schematic representation of the r.e.v. V. Among others, Ramesh et al. (1996) employed this geometry for the homogenization of the elastic properties of cement-based composites. It is indeed a special case of the n-layered inclusion model for which Hervé and Zaoui provided the elastic solution under deviatoric and volumetric loading at infinity (Hervé and Zaoui, 1993).

The different spheres are characterized by their radius, R_θ ($\theta \in [1,3]$, $1 =$ Inclusion (I), $2 =$ ITZ (i), $3 =$ matrix (m)); and the volume fractions of the different phases are given by ($R_0 = 0$):

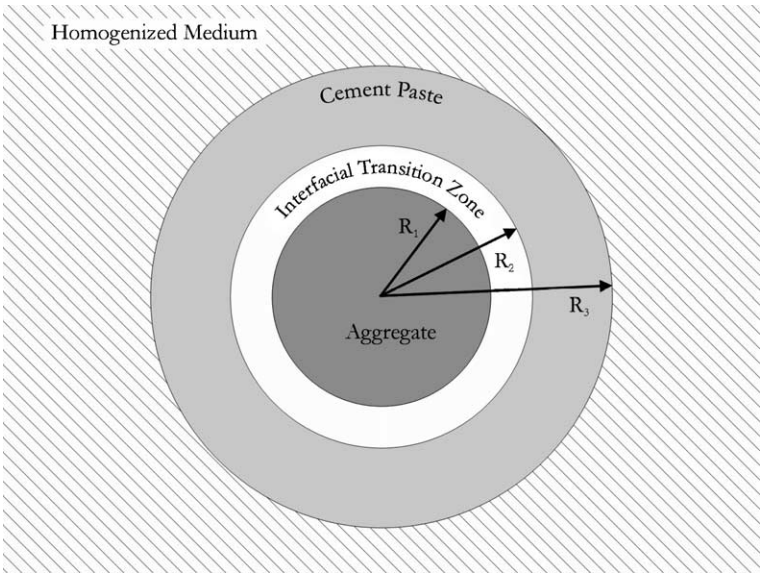

Fig. 3. Geometrical representation of the micromechanical model.

$$f_\theta = \frac{R_\theta^3 - R_{\theta-1}^3}{R_3^3}; \quad \frac{R_\theta}{R_3} = \sqrt[3]{\sum_{i=1}^{\theta} f_i}; \quad \theta \in [1,3] \tag{3}$$

where the reference volume is $V = \frac{4}{3}\pi R_3^3$. The volume of each individual phase is designated by V_θ. The three phases are considered to be homogeneous, and perfect bonding between the phases is assumed.

In addition to the geometrical representation, the strength properties in each phase are described by a microscopic strength criterion of the Drucker–Prager type (see Fig. 2):

$$\text{in } V_\theta : f(\underline{\underline{\sigma}}^\theta) = \sqrt{\frac{1}{2}} s^\theta + \delta_\theta \sigma_M^\theta - c_\theta \leqslant 0 \tag{4}$$

where c_θ is the microscopic cohesion and δ_θ is the microscopic; $s^\theta = \sqrt{\underline{\underline{s}}^\theta : \underline{\underline{s}}^\theta}$ is the 2nd deviator stress invariant of the microscopic stress tensor $\underline{\underline{\sigma}}^\theta = \underline{\underline{s}}^\theta + \sigma_M^\theta \underline{\underline{\delta}}$; and $\sigma_M^\theta = \frac{1}{3}\mathrm{tr}\underline{\underline{\sigma}}^\theta$ is the microscopic mean stress (1st stress invariant). The stress invariants can be linked to the strains by admitting, for monotonic loading, a non-linear elastic representation of the 'real' behavior of the phases up to failure:

$$s^\theta = 2\mu_\theta(\epsilon_\theta, \varepsilon_v^\theta)\epsilon_\theta; \quad \sigma_M^\theta = k_\theta(\epsilon_\theta, \varepsilon_v^\theta)\varepsilon_v^\theta \tag{5}$$

where μ_θ and k_θ are the secant shear and the secant bulk moduli of the microscopic phases, which are functions of the deviatoric strain invariant $\epsilon_\theta = \sqrt{\underline{\underline{\epsilon}}^\theta : \underline{\underline{\epsilon}}^\theta}$, $\underline{\underline{\epsilon}}^\theta(\underline{x}) = \underline{\underline{\varepsilon}}^\theta(\underline{x}) - \frac{1}{3}\varepsilon_v^\theta(\underline{x})\underline{\underline{\delta}}$, and the volumetric strain $\varepsilon_v^\theta = \mathrm{tr}\,\underline{\underline{\varepsilon}}^\theta$.

2.2. Localization: macroscopic, microscopic and effective strain quantities

The next step in the employed micromechanics approach relates to an appropriate definition of microscopic and macroscopic strain quantities, which allow the description of deformation of the composite and its phases. We consider an r.e.v. subjected to the displacement boundary conditions of the Hashin-type:

$$\text{on } \partial V : \underline{\xi}(\underline{x}) = \underline{\underline{E}} \cdot \underline{x} \tag{6}$$

where $\underline{\xi}$ is the microscopic displacement field; $\underline{x}$ denotes the position vector at the microscopic scale; and $\underline{\underline{E}}$ is the macroscopic strain in V, related to the microscopic strain $\underline{\underline{\varepsilon}}(\underline{x})$ by the volume averaging relation (see e.g. Zaoui, 2002):

$$\underline{\underline{E}} = \langle \underline{\underline{\varepsilon}}(\underline{x}) \rangle_V = \frac{1}{V} \int_V \underline{\underline{\varepsilon}}(\underline{x})\, \mathrm{d}V \tag{7}$$

Boundary condition (6) ensures that both macroscopic strain $\underline{\underline{E}}$ and microscopic strain $\underline{\underline{\varepsilon}}(\underline{x})$ are kinematically compatible. The premise of continuum micromechanics is that it is possible to separate the heterogeneous material into homogeneous phases associated with an on-average constant strain per phase. In linear elastic homogenization problems, this is achieved by means of a localization (or concentration) tensor, which concentrates the macroscopic strain $\underline{\underline{E}}$ into each phase $\underline{\underline{\varepsilon}}^\theta = \mathbb{A}_\theta : \underline{\underline{E}}$, where the 4th-order concentration tensor $\mathbb{A}_\theta$ is a function of elastic properties, and information relating to the morphology of the phases. By contrast, in non-linear micromechanics, the strain measurements serve primarily to study the deformation states close to failure. Therefore, we resort to 'effective' strain quantities, that are constant per phase. For isotropic materials, effective strain quantities are suitably developed as moments of the spatially varying microscopic strains $\underline{\underline{\varepsilon}}^\theta(\underline{x})$, induced by boundary condition (6) in each phase. The first moment delivers a suitable means of expressing the 'effective' volume strain per phase:

$$\bar{\varepsilon}_\theta = \mathrm{tr}\langle \underline{\underline{\varepsilon}}^\theta(\underline{x}) \rangle_{V_\theta} = \overline{A}_\theta^v E_v \tag{8}$$

where $\overline{A}^{v}_{\theta}$ links the macroscopic volume strain $E_v = \operatorname{tr}\underline{\underline{E}}$ to the effective volume strain $\bar{\varepsilon}_\theta$. The cohesive properties of composite materials refer to a material failure in shear that requires an appropriate introduction of effective shear strain quantities, constructed as moments of the spatially varying deviator strain tensor $\underline{\underline{\epsilon}}^{\theta}(\underline{x})$. The first moment of $\underline{\underline{\epsilon}}^{\theta}(\underline{x})$ reads:

$$\bar{\epsilon}_\theta = \sqrt{\langle \underline{\underline{\epsilon}}^{\theta}(\underline{x})\rangle_{V_\theta} : \langle \underline{\underline{\epsilon}}^{\theta}(\underline{x})\rangle_{V_\theta}} = \overline{A}^{d}_{\theta} E_d \tag{9}$$

where $E_d = \sqrt{\underline{\underline{E}}_d : \underline{\underline{E}}_d}$ is the 2nd deviator invariant of the macroscopic strain tensor $\underline{\underline{E}} = \underline{\underline{E}}_d + \frac{1}{3}E_v\underline{\underline{\delta}}$; and $\overline{A}^{d}_{\theta}$ links linearly the macroscopic applied strain E_d to the first moment effective deviator strain $\bar{\epsilon}_\theta$. Note that the linearity of the localization condition (9) is due to the fact that $\bar{\epsilon}_\theta$ is constructed from the volume averages of the strain tensor $\underline{\underline{\epsilon}}^{\theta}(\underline{x})$. By contrast, if the effective strain definition were to involve a higher order polynomial construction, i.e. higher moments of the strain tensor $\underline{\underline{\epsilon}}^{\theta}(\underline{x})$, the effective deviator strain can be shown to be a function of not only E_d, but also of other invariants of the macroscopic strain tensor $\underline{\underline{E}}$. For instance, the second moment of the deviator strain tensor obeys to the following form (Dormieux et al., 2002):

$$\bar{\bar{\epsilon}}^2_\theta = \langle \underline{\underline{\epsilon}}^{\theta}(\underline{x}) : \underline{\underline{\epsilon}}^{\theta}(\underline{x})\rangle_{V_\theta} = (\overline{\overline{A}}^{v}_{\theta})^2 E_v^2 + (\overline{\overline{A}}^{d}_{\theta})^2 E_d^2 \tag{10}$$

For the record, definition (9) of the effective deviator strain is often referred to as 'classical' secant method, and definition (10) as 'modified' secant method (Suquet, 1997); and the combination of (8) and (10) as 'mixed' secant method (Dormieux et al., 2002; Lemarchand et al., 2002). While further effective strain quantities can be defined as higher moments of the non-homogeneous microscopic strain field, we will restrict ourselves here to the two effective strain deviator invariants defined by (9) and (10) to study the effect of the interfacial properties on the cohesion of highly filled composites under pure deviator loading, for which $E_v = \bar{\varepsilon}_\theta = 0$. The two quantities which need to be determined are the localization factors $\overline{A}^{d}_{\theta}$ and $\overline{\overline{A}}^{d}_{\theta}$ required for the application of the classical and modified secant method. These concentration factors relate to the specific microscopic geometry under consideration. Dormieux et al. (2002) derived general expressions for these concentrations factors based on an energy argument (see application in Lemarchand et al. (2002)). Alternatively, as shown below, they can be determined from the analytical solution of the boundary value problem of the r.e.v. under consideration.

2.3. Homogenization

The third step of the non-linear homogenization approach relates to stresses, and the representation of the ultimate stress state close to failure by means of constitutive equations. Classically, the macroscopic stress $\underline{\underline{\Sigma}}$ is the volume average of the microscopic stresses $\underline{\underline{\sigma}}(\underline{x})$:

$$\underline{\underline{\Sigma}} = \langle \underline{\underline{\sigma}}(\underline{x})\rangle_V = \frac{1}{V}\int_V \underline{\underline{\sigma}}(\underline{x})\,\mathrm{d}V \tag{11}$$

Following experimental results [ ], the strength domain of the composite may be expressed by a Drucker–Prager type strength criteria (see Fig. 2):

$$\text{in } V : F(\underline{\underline{\Sigma}}) = \sqrt{\frac{1}{2}}S + \delta_{\hom}\Sigma_M - c_{\hom} \leqslant 0 \tag{12}$$

where $c_{\hom}$ is the macroscopic cohesion; $\delta_{\hom}$ is the macroscopic friction coefficient. The macroscopic stress invariants are linked to the strain invariants by a non-linear elastic representation of the material behavior:

$$S = 2\mu_{\hom}(E_v, E_d)E_d; \quad \Sigma_M = k_{\hom}(E_v, E_d)E_v \tag{13}$$

where μ_{hom} and k_{hom} are the macroscopic secant moduli of the composite. Furthermore, the microscopic stress invariants (5) can be rewritten as functions of the 'effective' strain quantities previously defined.

$$s^{\theta} = 2\mu_{\theta}(\epsilon_{\theta}^{\text{eff}}, \varepsilon_{\theta}^{\text{eff}})\epsilon_{\theta}^{\text{eff}}; \quad \sigma_{M}^{\theta} = k_{\theta}(\epsilon_{\theta}^{\text{eff}}, \varepsilon_{\theta}^{\text{eff}})\varepsilon_{\theta}^{\text{eff}} \tag{14}$$

where the effective deviatoric strain $\epsilon_{\theta}^{\text{eff}}$ and volumetric strain $\varepsilon_{\theta}^{\text{eff}}$ are defined respectively by either (9) or (10) and (8); two remarks:

(1) Focus of our study is the cohesive strength of the composite, that is a pure deviatoric loading for which $E_v = 0$. In addition, if we choose for the effective volumetric strain, the one given by the first moment (8), it is $\varepsilon_{\theta}^{\text{eff}} \equiv \bar{\varepsilon}_{\theta} = 0$ in pure deviatoric loading; and thus $\sigma_{M}^{\theta} = \Sigma_{M} = 0$. This reduces the non-linear elastic relations (14) and (13) to:

$$s^{\theta} = 2\mu_{\theta}(\epsilon_{\theta}^{\text{eff}})\epsilon_{\theta}^{\text{eff}}; \quad S = 2\mu_{\text{hom}}E_d \tag{15}$$

Given this assumption, the results developed below hold for the cohesion of a Drucker–Prager material, but also for the cohesion of a Von–Mises material.

(2) At failure, $f(\underline{\underline{\sigma}}^{m}) = 0$ and $F(\underline{\underline{\Sigma}}) = 0$, which corresponds to infinite values of the deviatoric strain invariants (except for rigid phases), $\epsilon_{\theta}^{\text{eff}} \to \infty$ and $E_d \to \infty$. Thus, for this limit case in pure deviatoric loading, a combination of the strength criteria (4) and (12) and the non-zero non-linear elastic constitutive relations (15) yields:

$$f(\underline{\underline{\sigma}}^{\theta}) = 0 \Longleftrightarrow \lim_{\epsilon_{\theta}^{\text{eff}} \to \infty} s^{\theta} = \sqrt{2}c_{\theta} \Rightarrow c_{\theta} = \sqrt{2} \lim_{\epsilon_{\theta}^{\text{eff}} \to \infty} [\mu_{\theta}(\epsilon_{\theta}^{\text{eff}})\epsilon_{\theta}^{\text{eff}}] \in]0; +\infty[\tag{16}$$

$$F(\underline{\underline{\Sigma}}) = 0 \Longleftrightarrow \lim_{E_d \to \infty} S = \sqrt{2}c_{\text{hom}} \Rightarrow c_{\text{hom}} = \sqrt{2} \lim_{E_d \to \infty} [\mu_{\text{hom}}E_d] \in]0; +\infty[\tag{17}$$

With (16) and (17) we arrived at reducing a strength problem of $\theta = 1, n$-phases and a composite to a problem per phase that involves only the ratios of the microscopic-to-macroscopic shear secant moduli and deviatoric strain invariants per phase:

$$\frac{c_{\text{hom}}}{c_{\theta}} = \lim_{\substack{E_d \to \infty \\ \epsilon_{\theta}^{\text{eff}} \to \infty}} \left[\frac{\mu_{\text{hom}}}{\mu_{\theta}(\epsilon_{\theta}^{\text{eff}})} \times \frac{E_d}{\epsilon_{\theta}^{\text{eff}}} \right] \tag{18}$$

The shear moduli ratio $\mu_{\text{hom}}/\mu_{\theta}$ can be addressed by means of a suitable linear homogenization scheme for the considered geometry; and the shear strain ratio $E_d/\epsilon_{\theta}^{\text{eff}}$ between the microscopic and macroscopic invariants through application of the effective strain quantities defined by relations (9) and (10). For a pure deviatoric loading, (18) reduces to:

$$\frac{c_{\text{hom}}}{c_{\theta}} = \lim_{\epsilon_{\theta}^{\text{eff}} \to \infty} \left(\frac{\mu_{\text{hom}}}{\mu_{\theta}(\epsilon_{\theta}^{\text{eff}})} \times \frac{1}{A_{\theta}^{d,\text{eff}}} \right) \tag{19}$$

where $A_{\theta}^{d,\text{eff}}$ is the concentration factor of the employed secant method (i.e. $\overline{A}_{\theta}^{d}$ or $\overline{\overline{A}}_{\theta}^{d}$). The limit (19) defines a set of n equations which are functions of the volume fractions and local elastic material properties. In addition, it defines $n - 1$ compatibility conditions between the strength properties of the phases, say ϑ and θ:

$$\frac{c_{\vartheta}}{c_{\theta}} = \eta \times \lim_{\substack{\epsilon_{\vartheta}^{\text{eff}} \to \infty \\ \epsilon_{\theta}^{\text{eff}} \to \infty}} \left(\frac{A_{\vartheta}^{d,\text{eff}}}{A_{\theta}^{d,\text{eff}}} \right) \tag{20}$$

where $\eta = \mu_\vartheta/\mu_\theta$ is the shear moduli ratio between the two phases. Last, for the solution of the limit problem (19) and (20), note that an infinite shear strain $\epsilon_\theta^{\text{eff}} \to \infty$, in terms of a secant modulus, is equivalent to $\mu_\theta \to 0$. Thus, at failure, $\mu_\vartheta \to 0$ and $\mu_\theta \to 0$. But the ratio $\eta = \mu_\vartheta/\mu_\theta$ is assumed to remain fixed, and actually substitutes for the cohesion ratio c_ϑ/c_θ according to (20). Thus, a combination of (19) and (20) closes the non-linear homogenization approach of strength properties, relating the composite cohesion to the microscopic cohesion of the involved phases.

2.4. Application of Hervé–Zaoui's BVP-Solution

Relations (19) and (20) are general expressions for the homogenization of cohesive properties of isotropic composite materials. Application to a particular geometry requires choice of an appropriate linear upscaling scheme. The linear elastic solution for an n-layered inclusion model is due to Hervé and Zaoui (1993), which we employ for the 3-layered composite material system displayed in Fig. 3. Given the restriction to a purely deviatoric loading, we consider the Hervé–Zaoui solution for an r.e.v. subjected at infinity to a uniform deviatoric loading:

$$\text{on } \partial V : \underline{\xi}(\underline{x}) = \underline{\underline{E}}^d \cdot \underline{x} \tag{21}$$

The solution of the boundary value problem for the 3-layered inclusion model, detailed in Table 2, gives the spatially varying deviator strain tensor $\underline{\underline{\epsilon}}^\theta(\underline{x})$ as linear function of the macroscopic deviator strain $\underline{\underline{E}}^d$. Use of the Hervé–Zaoui strain solution $\underline{\underline{\epsilon}}^\theta(\underline{x})$ in (9) and (10) gives explicit expressions for the localization factors $\overline{A}_\theta^d$ and $\overline{\overline{A}}_\theta^d$, which are functions of the interface-matrix shear modulus ratio $\eta_i = \mu_i/\mu_m$ and $\eta_I = \mu_I/\mu_m$; the shear-to-bulk modulus ratio of matrix and interface, $\rho_\theta = \mu_\theta/k_\theta$, and of the volume fractions f_θ:

$$\overline{A}_\theta^d = \sqrt{\frac{\langle \underline{\underline{\epsilon}}^\theta(\underline{x}) \rangle_{V_\theta} : \langle \underline{\underline{\epsilon}}^\theta(\underline{x}) \rangle_{V_\theta}}{\underline{\underline{E}}^d : \underline{\underline{E}}^d}} = \overline{A}_\theta^d(\eta_I, \eta_i, \rho_\theta, f_\theta) \tag{22}$$

$$\overline{\overline{A}}_\theta^d = \sqrt{\frac{\langle \underline{\underline{\epsilon}}^\theta(\underline{x}) : \underline{\underline{\epsilon}}^\theta(\underline{x}) \rangle_{V_\theta}}{\underline{\underline{E}}^d : \underline{\underline{E}}^d}} = \overline{\overline{A}}_\theta^d(\eta_I, \eta_i, \rho_\theta, f_\theta) \tag{23}$$

The concentration factors $\overline{A}_\theta^d$ and $\overline{\overline{A}}_\theta^d$, which are given in Appendix A, are the sole quantities required to solve the limit problem (19). More precisely, following 'classical' linear homogenization theories, the composite shear modulus μ_{hom} for the 3-phase composite model with rigid inclusions ($\bar{\epsilon}_I = 0 \Longleftrightarrow \overline{A}_I^d = 0$) is given by (see detailed derivation in Appendix B):

$$\frac{\mu_{\text{hom}}}{\mu_m} = \lim_{\eta_I \to \infty} (\eta_I + (1-\eta_I) f_m \overline{A}_m^d + (\eta_i - \eta_I) f_i \overline{A}_i^d) \tag{24}$$

Use of (24) in (19) yields a first homogenization expression for the macroscopic cohesion:

$$\frac{c_{\text{hom}}}{c_m} = \lim_{\substack{\eta_I \to \infty \\ \rho_m \to 0}} \lim_{\rho_i \to 0} \left(\frac{\eta_I + (1-\eta_I) f_m \overline{A}_m^d + (\eta_i - \eta_I) f_i \overline{A}_i^d}{A_m^{d,\text{eff}}} \right) = \mathscr{F}(\eta_i; f_\theta) \tag{25}$$

Evaluated for the limit case $\epsilon_m^{\text{eff}} \to \infty$ and $\epsilon_i^{\text{eff}} \to \infty$, which is equivalent to $\rho_m = \mu_m/k_m \to 0$ and $\rho_i = \mu_i/k_i \to 0$, expression (25) depends only on the interface-to-shear modulus ratio $\eta_i = \mu_i/\mu_m$ and the volume fractions f_θ. The final step in the homogenization approach then consists of replacing the interface-to matrix shear modulus ratio $\eta_i = \mu_i/\mu_m$ in (25) by the interface-to-matrix cohesion ratio $\chi_i = c_i/c_m$; that is from (24):

Table 2
Hervé–Zaoui's solution for deviatoric displacement loading at infinity (Hervé and Zaoui, 1993)

Hervé–Zaoui solution for deviatoric displacement at infinity
The components of the displacement field in the r.e.v. read in spherical coordinates

$$\xi_r^{(\theta)} = U_r^{(\theta)}(r)\sin^2\psi\cos 2\phi$$

$$\xi_\psi^{(\theta)} = U_\psi^{(\theta)}(r)\sin\psi\cos\psi\cos 2\phi$$

$$\xi_\phi^{(\theta)} = U_\phi^{(\theta)}(r)\sin\psi\sin 2\phi$$

with

$$\begin{pmatrix} U_r^{(\theta)} \\ U_\psi^{(\theta)} \\ U_\phi^{(\theta)} \end{pmatrix} = \begin{bmatrix} r & -\frac{6\nu_\theta}{1-2\nu_\theta}r^3 & \frac{3}{r^4} & \frac{5-4\nu_\theta}{1-2\nu_\theta}\frac{1}{r^2} \\ r & -\frac{7-4\nu_\theta}{1-2\nu_\theta}r^3 & -\frac{2}{r^4} & \frac{2}{r^2} \\ -r & \frac{7-4\nu_\theta}{1-2\nu_\theta}r^3 & \frac{2}{r^4} & -\frac{2}{r^4} \end{bmatrix} \begin{pmatrix} a_\theta \\ b_\theta \\ c_\theta \\ d_\theta \end{pmatrix}$$

The constants a_θ, b_θ, c_θ and d_θ are determined through four independent displacement and stress continuity conditions between the phases. These conditions are written in the compact form: $\mathbf{L}_\theta(R_\theta)\cdot\mathbf{W}_\theta = \mathbf{L}_{\theta+1}(R_{\theta+1})\cdot\mathbf{W}_{\theta+1}$
where $\mathbf{W}_\theta = [\,a_\theta \quad b_\theta \quad c_\theta \quad d_\theta\,]^{\mathrm{T}}$, and $\mathbf{L}_\theta(r)$ is given by:

$$\mathbf{L}_\theta(r) = \begin{bmatrix} r & -\frac{6\nu_\theta}{1-2\nu_\theta}r^3 & \frac{3}{r^4} & \frac{5-4\nu_\theta}{1-2\nu_\theta}\frac{1}{r^2} \\ r & -\frac{7-4\nu_\theta}{1-2\nu_\theta}r^3 & -\frac{2}{r^4} & \frac{2}{r^2} \\ \mu_\theta & \frac{3\nu_\theta}{1-2\nu_\theta}\mu_\theta r^2 & -\frac{12}{r^5}\mu_\theta & \frac{2(\nu_\theta-5)}{1-2\nu_\theta}\frac{\mu_\theta}{r^3} \\ \mu_\theta & -\frac{7+2\nu_\theta}{1-2\nu_\theta}\mu_\theta r^2 & \frac{8}{r^5}\mu_\theta & 2\frac{1+\nu_\theta}{1-2\nu_\theta}\frac{\mu_\theta}{r^3} \end{bmatrix}$$

The previous relations allow the successive determination of the constants in layer $\theta+1$ from the one determined before in layer θ:

$$\mathbf{W}_{\theta+1} = \mathbf{M}^{(\theta)}\cdot\mathbf{W}_\theta; \quad \mathbf{M}^{(\theta)} = \mathbf{L}_{\theta+1}^{-1}(R_\theta)\cdot\mathbf{L}_\theta(R_\theta)$$

This gives the possibility to express all unknown coefficients with respect to phase 1:

$$\mathbf{W}_{\theta+1} = \mathbf{P}^{(\theta)}\cdot\mathbf{W}_1; \quad \mathbf{P}^{(\theta)} = \prod_{j=1}^{\theta}\mathbf{M}^{(j)}(R_j)$$

Carrying out this operation for the three layered inclusion delivers the following explicit solution for the sought constants:

$$\mathbf{W}_\theta = \begin{pmatrix} a_\theta \\ b_\theta \\ c_\theta \\ d_\theta \end{pmatrix} = \frac{E^d}{\sqrt{2}\left(P_{22}^{(3)}P_{11}^{(3)} - P_{12}^{(3)}P_{21}^{(3)}\right)}\mathbf{P}^{(\theta-1)}\cdot\begin{pmatrix} P_{22}^{(3)} \\ -P_{21}^{(3)} \\ 0 \\ 0 \end{pmatrix}$$

Given the linearity of $\mathbf{W}_\theta$ with respect to E^d, it is convenient to work with the normalized constants $\overline{\mathbf{W}}_\theta = \mathbf{W}_\theta/E^d = [\,\bar{a}_\theta \quad \bar{b}_\theta \quad \bar{c}_\theta \quad \bar{d}_\theta\,]^{\mathrm{T}}$
With the solution for $\underline{\xi}^{(\theta)}$, the microscopic strains follow:

$$\underline{\underline{\epsilon}}^{\theta}(\underline{x}) = \frac{1}{2}\left(\nabla\underline{\xi}^{(\theta)} + {}^{t}\nabla\underline{\xi}^{(\theta)}\right)$$

The localization factors are obtained with (22) and (23) and are given in Appendix A

$$\chi_i^{\text{eff}} = \frac{c_i}{c_m} = \eta_i \times \lim_{\substack{\rho_m \to 0 \\ \rho_i \to 0}} \left(\frac{A_i^{d,\text{eff}}}{A_m^{d,\text{eff}}} \right) \tag{26}$$

This variable change $\eta_i \to \chi_i^{\text{eff}}$ is secant method specific. For the classical secant method, for which $\langle \bar{\epsilon}_\theta \rangle_V = E_d \Longleftrightarrow \langle \overline{A}_\theta^d \rangle_V = 1$, Eq. (26) can be evaluated from:

$$\chi_i^{\text{eff}} \equiv \bar{\chi}_i = \eta_i \times \lim_{\substack{\rho_m \to 0 \\ \rho_i \to 0}} \left(\frac{1 - f_m \overline{A}_m^d}{f_i \overline{A}_m^d} \right) \tag{27}$$

On the other hand, for the modified secant method, for which $\langle \bar{\bar{\epsilon}}_\theta \rangle_V \neq E_d$, the concentration factors for the interface $A_i^{d,\text{eff}} \equiv \overline{\overline{A}}_i^d$ and for the matrix $A_m^{d,\text{eff}} \equiv \overline{\overline{A}}_m^d$ need to be evaluated from (23) [see Appendix A]. Use of this variable change in (26) then delivers a second definition of the composite cohesion as function of the cohesion ratio $\chi_i^{\text{eff}} \equiv \bar{\bar{\chi}}_i$, which substitutes for η_i into the homogenization solution (25):

$$\frac{c_{\text{hom}}}{c_m} = \mathscr{F}(\eta_i \to \chi_i^{\text{eff}}; f_\theta) = \mathscr{G}(\chi_i^{\text{eff}}; f_\theta) \tag{28}$$

Expression (28) does not permit an analytical expression. But using the step-by-step calculation procedure described here above, the problem is straightforwardly solved with any symbolic mathematical software.

3. Discussion

3.1. Parameter study: the effect of the interface cohesion on the composite cohesion

For a fixed inclusion volume fraction of $f_I = 0.5$, Figs. 4–6 display the results obtained with the strength homogenization model for three interface volume fractions $f_i = 0.15; 0.30; 0.45$. For both the classical and the modified secant methods, the figures illustrate the successive results of the homogenization procedure:

- The "a"-figures display the cohesive ratio as a function of the shear-modulus ratio $\eta \in [0, 1]$, where for convenience we dropped the subscript "i". It is interesting to note that the classical and modified secant method do not deliver the same solution, and diverge even for high interface volume fractions (see Fig. 6a). This is readily understood from the fact that when the interface volume fraction tends toward 0.5, the matrix vanishes, for $f_I = 0.5$, and the representation as a three phase model becomes obsolete.
- The "b"-figures display the relation between η and χ. It is interesting to note here, that for low values of $\eta \leqslant 0.2$, both secant methods deliver almost identical values. Note also that the interface-to-matrix cohesion range of interest is $\chi \in [0, 1]$, which corresponds to η-values roughly smaller than 0.5. Higher values for χ are theoretically possible, but practically difficult to achieve, requiring specific surface treatment of the inclusions, to achieve a higher interface cohesion than the matrix.
- Finally, the "c"-figures display the actual result of the homogenization procedure, that is c_{hom}/c_m as a function of the interface-to-matrix cohesion ratio $\chi \in [0, 1]$, obtained by the variable change $\eta \to \chi$. In all the considered cases, it appears that the macroscopic cohesion ratio is a non-linear increasing function of the interface-to-matrix cohesion ratio. The classical secant method generally predicts a higher composite cohesion than the modified secant method. But what is interesting to note is that there exists a critical value of the interface-to-matrix cohesion ratio χ, below which the composite cohesion is smaller than the one of the matrix, i.e. $c_{\text{hom}}/c_m < 1$; and above this value it is the inverse. Fig. 7 displays this critical interface-to-matrix cohesion ratio, $\chi^{\text{crit}} \Longleftrightarrow c_{\text{hom}}/c_m = 1$, as a function of the interface volume

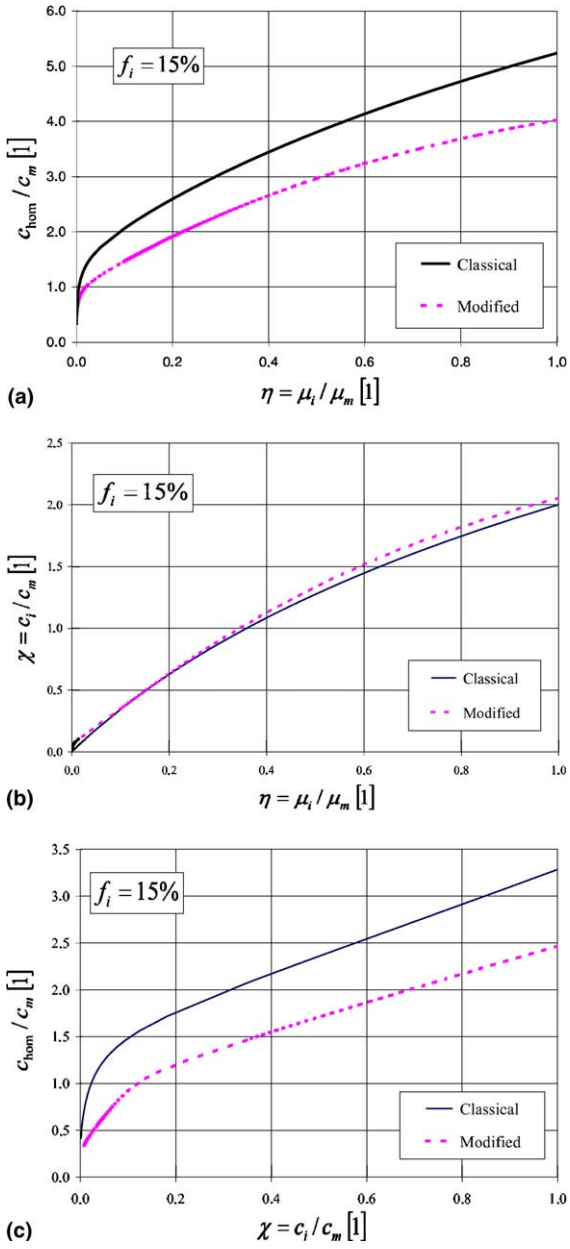

Fig. 4. Strength homogenization procedure for $f_i = 0.15$ and $f_I = 0.5$: (a) c_{hom}/c_m vs. η; (b) χ vs. η; (c) c_{hom}/c_m vs. $\chi = c_i/c_m$.

fraction f_i for an inclusion volume fraction of $f_I = 0.5$. As expected, a higher interface volume fraction requires compensation by a higher χ^{crit}-value to deliver the same performance $c_{\text{hom}}/c_m = 1$. Interestingly, the modified secant method delivers, for moderate interface volume fractions, an almost linear χ^{crit}-f_i relation, with values that are much greater than the one predicted by the classical secant method. This highlights that the modified secant method is more sensitive to the interface properties than the classical secant method.

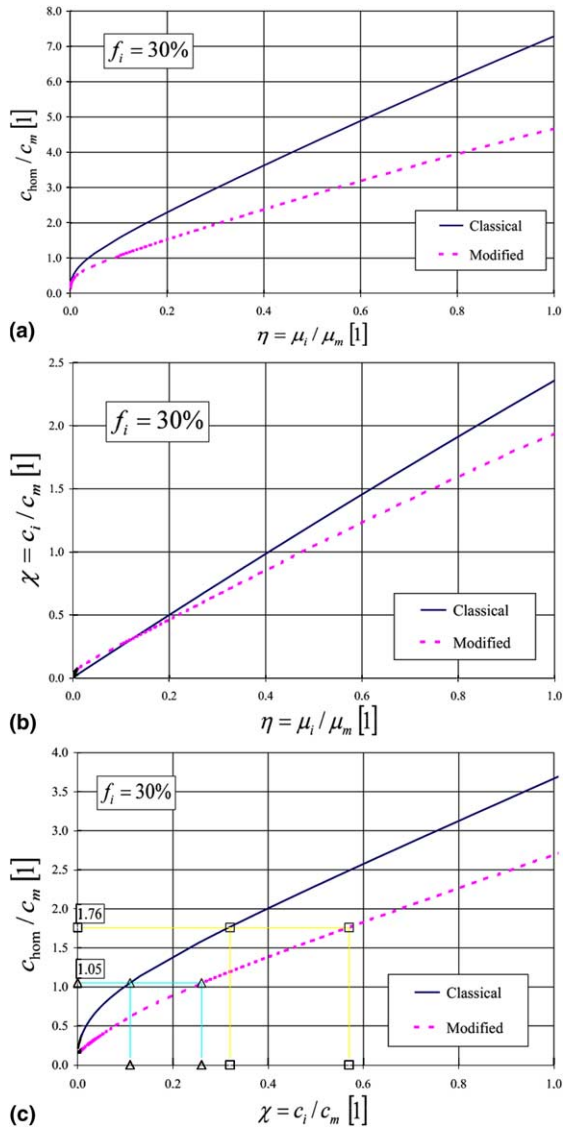

Fig. 5. Strength homogenization procedure for $f_i = 0.30$ and $f_I = 0.5$: (a) c_{hom}/c_m vs. η; (b) χ vs. η; (c) c_{hom}/c_m vs. $\chi = c_i/c_m$.

3.2. Inverse analysis: chemical softening of interface cohesion

It is interesting to perform an inverse analysis of the interface cohesion properties for the experimental values of non-degraded and degraded cement paste materials given in Table 1. The input parameter to the inverse application of the model are:

(1) The volume fractions of the inclusion and the interface. The first is known, $f_I = 0.5$, the second can be determined from (3). In the mortar, the aggregate size is assumed to be uniform of roughly $R_1 = 0.2\,\text{mm}$. Furthermore, the SEM micrograph (Fig. 1) of the chemically degraded material shows

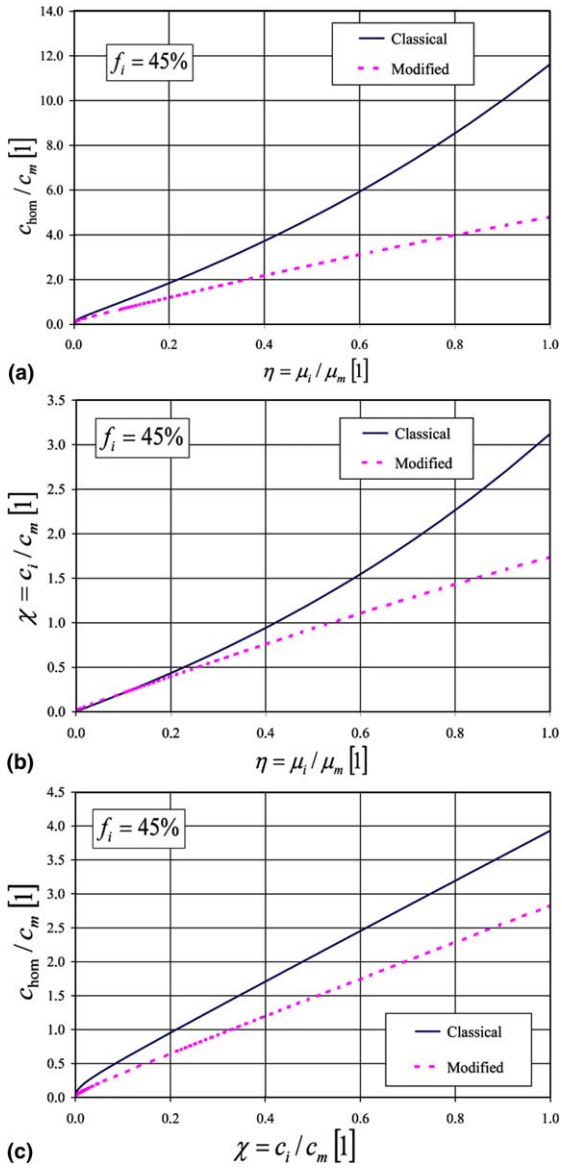

Fig. 6. Strength homogenization procedure for $f_i = 0.45$ and $f_I = 0.5$: (a) c_{hom}/c_m vs. η; (b) χ vs. η; (c) c_{hom}/c_m vs. $\chi = c_i/c_m$.

that the ITZ size is limited approximately to $D_i \simeq 20\,\mu\text{m}$, which is on the same order of typical ITZ sizes of 10–40 μm, reported for cementitious materials in the open literature (see for example Maso, 1996; Monteiro and Ostertag, 1989). Thus, for the mortar under consideration, $f_i \simeq 0.3$.

(2) The experimental mortar-to-cement paste cohesion ratio is $c_{\text{hom}}/c_m = 1.76$ for the non-degraded material, and $c_{\text{hom}}/c_m = 1.05$ for the chemically softened material.

Using these values in Fig. 5c ($f_i = 0.3$; $f_I = 0.5$) provides a means of estimating the interface-to-matrix cohesion ratio $\chi = c_i/c_m$. For the non-degraded material, we obtain:

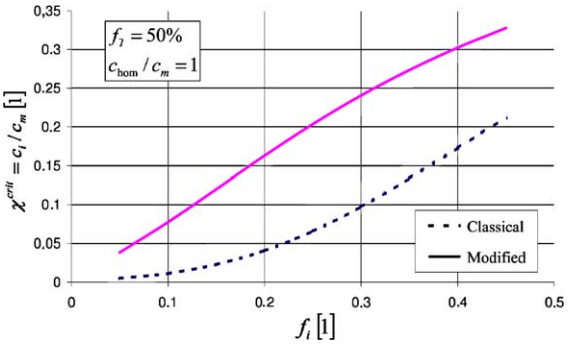

Fig. 7. Critical interface-to-matrix cohesion ratio $\chi^{\text{crit}} \Longleftrightarrow c_{\text{hom}}/c_m = 1$ vs. interface volume fraction ($f_I = 0.5$).

$$\left(\frac{c_{\text{hom}}}{c_m}\right)^{0} = 1.76 \Rightarrow \chi^0 \in [0.32; 0.57] \tag{29}$$

where the lower value corresponds to the classical secant method and the upper value to the modified secant method. Analogously, for the degraded material:

$$\left(\frac{c_{\text{hom}}}{c_m}\right)^{\infty} = 1.05 \Rightarrow \chi^\infty \in [0.11; 0.26] \tag{30}$$

The values for the non-degraded material (29) are on the same order of reported microhardness measurements of the ITZ (Mehta and Monteiro, 1988; Yuji, 1988). But, in addition, the model provides a means of estimating the effect of chemical leaching on the interface cohesion, for which both methods converge to a residual interface cohesion of approximately 15% of the initial cohesion:

$$\frac{c_i^\infty}{c_i^0} = \frac{\chi^\infty}{\chi^0} \times \frac{c_m^\infty}{c_m^0} \in [0.13; 0.17] \tag{31}$$

This chemical softening of the interface is much larger than the bulk matrix softening of $c_m^\infty/c_m^0 = 0.38$, and highlights the particular effect of chemical softening on the interface cohesion. It signifies that beyond the overall strength loss due to calcium leaching, a particularly weak interface exists in chemically softened cement-based material that dominates the cohesion of the composite material. The microstructural appearance as shown in the SEM graph (Fig. 1) underlines this finding with the large pores and high porosity.

3.3. Limit case of porous matrix

By means of a similar inverse analysis, the model provides a way to distinguish the intrinsic chemical softening of the solid phase of the matrix from the chemical softening induced by an increase of the porosity of the cement paste. To this end, we inspect the cohesion homogenization model for the limit of empty inclusions, for which $c_i = 0$, or $\eta_i = \chi_i = 0$. In this case, the only mechanically active phase is the matrix of volume fraction $f_m = 1 - \phi$, where ϕ is the porosity. For this two phase composite, (25) reduces to:

$$\frac{c_{\text{hom}}}{c_m} = f_m \lim_{\rho_m \to 0} \left(\frac{\overline{A}_m^d}{A_m^{d,\text{eff}}}\right) \tag{32}$$

The classical secant method ($A_m^{d,\text{eff}} = \overline{A}_m^d$) delivers a linear relation between the cohesion ratio c_{hom}/c_m and the solid volume fraction f_m. By contrast, the modified secant method delivers a non-linear relation between the cohesion ratio and the matrix volume fraction:

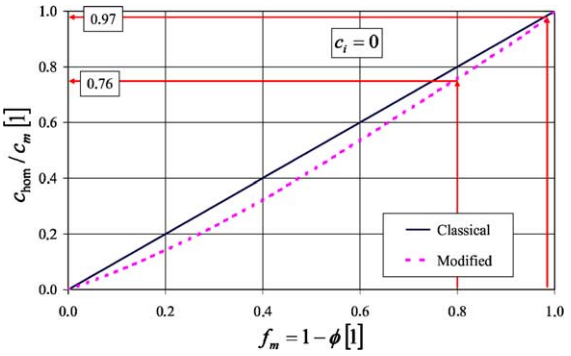

Fig. 8. Limit Case of empty inclusions: c_{hom}/c_m vs. f_m (= solid volume fraction).

$$\chi_i = 0 : \frac{\overline{\overline{c_{\text{hom}}}}}{c_m} = f_m \lim_{\rho_m \to 0} \left(\frac{\overline{A_m^d}}{\overline{\overline{A_m^d}}} \right) = \mathscr{H}(f_m) \tag{33}$$

Function $\mathscr{H}(f_m)$ is displayed in Fig. 8. For the inverse application, we note that $1 - f_m$ corresponds to the porosity, $c_{\text{hom}} = c_m$ is the cement paste cohesion, and $c_\theta = c_s$ is the unknown cohesion of the matrix solid phase (C-S-H, Portlandite, etc.). For the classical secant method, using the values of Table 1, we obtain:

$$\frac{\overline{c_s^\infty}}{c_s^0} = \left(\frac{c_m^\infty}{c_m^0} \right) \times \frac{f_m^0}{f_m^\infty} = 0.46 \tag{34}$$

Analogously, for the modified secant method:

$$\frac{\overline{\overline{c_s^\infty}}}{c_s^0} = \left(\frac{c_m^\infty}{c_m^0} \right) \times \frac{\mathscr{H}(f_m^0)}{\mathscr{H}(f_m^\infty)} = 0.48 \tag{35}$$

where $\mathscr{H}(f_m^0) = 0.97$ and $\mathscr{H}(f_m^\infty) = 0.76$ are the values taken by function $\mathscr{H}(f_m)$ displayed in Fig. 8 for respectively the initial porosity $1 - f_m^0 = 0.03$ and the asymptotic porosity $1 - f_m^\infty = 0.21$ of the cement paste. It therefore appears, from the inverse application of the non-linear homogenization model, that calcium leaching leads to an intrinsic softening of the solid cohesion of the matrix of more than 50%. This highlights that calcium leaching does not only affect the strength properties by an increase of the porosity, but as well by an intrinsic softening of the solid material composing the matrix.

3.4. Extension to account for aggregate grading

In the case of the tested mortar, the grading of the aggregates is very narrow and a simplified calculation suffices to obtain the ITZ volume fraction. For commonly used concretes the calculation of the ITZ volume fraction has to be improved. In general, the grading of the aggregates is known and can be described as a function $r = r(m)$ obtained in standard sieve curves. In this function r is the radius of the aggregate and m the mass percentage of aggregates that has a smaller radius than r. With such a grading curve at hand, the volume fraction of the ITZ, f_i, assuming that the ITZ has a constant size, D, and the aggregates have a uniform density, can be estimated according to:

$$\frac{f_i}{f_I} = \int_0^1 \frac{V_{\text{ITZ}}}{V_i} \mathrm{d}m = \int_0^1 \left[\left(1 + \frac{D}{r(m)} \right)^3 - 1 \right] \mathrm{d}m \tag{36}$$

where f_I is the total volume fraction of the aggregates. This provides a means of employing the model to concrete and mortar with different aggregate volume fractions and size distributions.

4. Conclusions

The non-linear homogenization procedure developed in this paper provides a quantitative means of studying the role of interface properties on the macroscopic cohesion of highly filled composite materials:

(1) The two key elements for upscaling strength properties are (1) the separation of the heterogeneous material system in phases of constant strength properties, and (2) the definition of appropriate effective strain quantities that capture the morphological features of the microstructure. For the considered three phase inclusion geometry, a higher order moment definition of the effective strain (i.e. modified secant method) is more sensitive to the interface properties than a first order moment definition (i.e. classical secant method). This leads, in general, to lower composite strength values.
(2) There exists a critical interface-to-matrix cohesion ratio $\chi^{\text{crit}} = c_i/c_m$ below which the presence of an interface weakens the composite cohesion compared to the matrix cohesion. This ratio χ^{crit} depends only on the interface and inclusion volume ratio; it appears therefore to be rather related to the micro-geometry of the composite, than to strength properties. Sound composite materials have typical interface-to-matrix cohesion ratio that are much higher than this critical value. In turn, chemically softened materials come very close to this critical value, $c_{\text{hom}}/c_m \to 1$. This critical interface-to-matrix cohesion ratio χ^{crit} may serve as a design parameter for an efficient design of such composite materials.
(3) The inverse application of the model provides conclusive evidence that chemical degradation of cement-based materials does affect the mechanical performance of the composite not only through a change of volume proportions (i.e. increase of porosity), but as well through a chemical softening of the solid's cohesion. This important result needs still to be confirmed by advanced micro-to-nano mechanical testing (e.g. nanoindentation; see Constantinides and Ulm, 2002). For mortar, it turns out that the interface strength properties are far more affected than the cement paste matrix. This is consistent with the fact that the ITZ has in general a higher porosity, and thus is more exposed to chemical attack than the matrix.

Acknowledgment

This research was performed as part of Grant No. DE-FG03-99SF21891/A000 of the US Department of Energy (DOE) to MIT. The authors gratefully acknowledge the support of this work by the Nuclear Energy Research Initiative Program of DOE. The project benefits from a close cooperation with Prof. Luc Dormieux, Ecole Nationale des Ponts et Chaussées, France, and with Dr. Jérôme Sercombe, C.E.A. Saclay, France.

Appendix A. Concentration factors

The concentration factors of the Hervé–Zaoui scheme are determined by using the microscopic strain solution in (9) and (10). This delivers the following explicit expressions:

$$\overline{A}_\theta^d = \frac{\bar{\epsilon}_\theta}{E_d} = \sqrt{2}\left(\bar{a}_\theta - \frac{21\bar{b}_\theta}{5(1-2\nu_\theta)} \times \frac{R_\theta^5 - R_{\theta-1}^5}{R_\theta^3 - R_{\theta-1}^3}\right) \tag{A.1}$$

$$(\overline{\overline{A}}^{d}_{\theta})^2 = (\bar{\bar{\epsilon}}_{\theta}/E_d)^2 = \frac{1}{(1-2\nu_{\theta})^2}\left[3\bar{b}_{\theta}^2(8\nu_{\theta}^2+35)\frac{R_{\theta}^7-R_{\theta-1}^7}{R_{\theta}^3-R_{\theta-1}^3} + 42\bar{a}_{\theta}\bar{b}_{\theta}(2\nu_{\theta}-1)\frac{R_{\theta}^5-R_{\theta-1}^5}{R_{\theta}^3-R_{\theta-1}^3} + 5\bar{a}_{\theta}^2(1-2\nu_{\theta})^2\right.$$
$$+24\bar{b}_{\theta}\bar{d}_{\theta}\nu_{\theta}(5-7\nu_{\theta})\frac{R_{\theta}^2-R_{\theta-1}^2}{R_{\theta}^3-R_{\theta-1}^3} + 8\bar{d}_{\theta}^2(7\nu_{\theta}^2-10\nu_{\theta}+10)\frac{1}{R_{\theta}^3R_{\theta-1}^3}$$
$$\left.+144\bar{c}_{\theta}\bar{d}_{\theta}(1-2\nu_{\theta})\frac{R_{\theta}^5-R_{\theta-1}^5}{R_{\theta}^5R_{\theta-1}^5(R_{\theta}^3-R_{\theta-1}^3)} + 120\bar{c}_{\theta}^2(1-2\nu_{\theta})^2\frac{R_{\theta}^7-R_{\theta-1}^7}{R_{\theta}^7R_{\theta-1}^7(R_{\theta}^3-R_{\theta-1}^3)}\right] \tag{A.2}$$

where ν_{θ} denotes the Poisson ratio of phase θ; and $\bar{a}_{\theta} = a_{\theta}/E_d$, $\bar{b}_{\theta} = b_{\theta}/E_d$, $\bar{c}_{\theta} = c_{\theta}/E_d$, and $\bar{d}_{\theta} = d_{\theta}/E^d$ are the normalized constants of the Hervé–Zaoui displacement solution (see Table 2).

Appendix B. Composite shear modulus

This appendix shows the derivation of expression (24) of the composite shear modulus which can be extracted from the general Hervé–Zaoui solution.

Following 'classical' linear homogenization theory, the composite shear modulus is determined from the application of the stress volume average condition (11) together with a linear elastic constitutive law for the 3-phase composite inclusion model:

$$\underline{\underline{S}} = \langle \underline{\underline{s}} \rangle_V = \langle 2\mu_{\theta}\underline{\underline{\epsilon}}^{\theta}(\underline{x})\rangle_V = 2\mu_m f_m \underline{\underline{\bar{\epsilon}}}_m + 2\mu_i f_i \underline{\underline{\bar{\epsilon}}}_i + 2\mu_I f_I \underline{\underline{\bar{\epsilon}}}_I = 2\mu_{\text{hom}}\underline{\underline{E}}^d \tag{B.1}$$

where $\underline{\underline{\bar{\epsilon}}}_{\theta} = \langle \underline{\underline{\epsilon}}^{\theta}(\underline{x})\rangle_{V_{\theta}}$ denote the volume average of the deviator strain tensor in the phases, which are related by the strain compatibility condition:

$$f_m \underline{\underline{\bar{\epsilon}}}_m + f_i \underline{\underline{\bar{\epsilon}}}_i + f_I \underline{\underline{\bar{\epsilon}}}_I = \underline{\underline{E}}^d \tag{B.2}$$

For the specific n-layered inclusion geometry Hervé and Zaoui (1993) showed that $\underline{\underline{\bar{\epsilon}}}_{\theta} = \overline{\overline{A}}^{d}_{\theta}\underline{\underline{E}}^d$, which leads to the following expression of the composite shear modulus:

$$\mu_{\text{hom}} = \mu_m f_m \overline{\overline{A}}^{d}_{m} + \mu_i f_i \overline{\overline{A}}^{d}_{i} + \mu_I f_I \overline{\overline{A}}^{d}_{I} \tag{B.3}$$

This is the general linear elastic expression for a composite composed of three deformable inclusions, for which $\overline{\overline{A}}^{d}_{\theta}$ is given by (A.1). For rigid inclusions, for which $\mu_I \to \infty$ and $\underline{\underline{\bar{\epsilon}}}_I \to 0$, (B.3) needs to be evaluated for an infinite inclusion shear modulus:

$$\left.\frac{\mu_{\text{hom}}}{\mu_m}\right|_{\eta_I\to\infty} = \lim_{\eta_I\to\infty}(f_m\overline{\overline{A}}^{d}_{m}(1-\eta_I) + (\eta_i-\eta_I)f_i\overline{\overline{A}}^{d}_{i}) \tag{B.4}$$

where $\eta_i = \mu_i/\mu_m$ and $\eta_I = \mu_I/\mu_m$. For a two phase material composed of matrix and empty inclusions, $\eta_I = 0$ and $f_I\overline{\overline{A}}^{d}_{I} = 1 - f_m\overline{\overline{A}}^{d}_{m}$

$$\left.\frac{\mu_{\text{hom}}}{\mu_m}\right|_{\eta_I=0} = f_m\overline{\overline{A}}^{d}_{m} \tag{B.5}$$

Finally, for a two phase composite composed of matrix and rigid inclusions, $\eta_I \to \infty$ and $f_I\overline{\overline{A}}^{d}_{I} = 1 - f_m\overline{\overline{A}}^{d}_{m}$:

$$\left.\frac{\mu_{\text{hom}}}{\mu_m}\right|_{\eta_I\to\infty} = \lim_{\eta_I\to\infty}(\eta_I + (1-\eta_I)f_m\overline{\overline{A}}^{d}_{m}) \tag{B.6}$$

References

Consoli, N.C., Prietto, D.M., Ulbrich, L.A., 1998. Influence of fiber and cement addition on behavior of sandy soil. Journal of Geotechnical and Geoenvironmental Engineering 124 (12), 1211–1214.

Constantinides, G., Ulm, F.-J., 2002. The effect of two types of C-S-H on the elasticity of cementbased materials: results from nanoindentation and micromechanical modeling. Cement and Concrete Research 34 (1), 67–80.

Dormieux, L., Molinari, A., Kondo, D., 2002. Micromechanical approach to the behavior of poroelastic materials. Journal of the Mechanics and Physics of Solids, 2203–2231.

Garboczi, E.J., Berryman, J.G., 2001. Elastic moduli of a material containing composite inclusions: effective medium theory and finite element computations. Mechanics of Materials 33 (8), 455–470.

Hashin, Z., Monteiro, P.J.M., 2002. An inverse method to determine the elastic properties of the interphase between the aggregate and the cement paste. Cement an Concrete Research 32, 1291–1300.

Hervé, E., Zaoui, A., 1993. *n*-layered inclusion-based micromechanical modelling. International Journal of Engineering Science 31 (1), 1–10.

Heukamp, F.H., Ulm, F.-J., Germaine, J.T., 2001a. Mechanical properties of calcium leached cement pastes: triaxial stress states and the influence of the pore pressure. Cement and Concrete Research 31 (5), 767–774.

Heukamp, F.H., Ulm, F.-J., Germaine, J.T., 2001b. Poroplastic properties of calcium leached cement-based materials. Cement and Concrete Research 33 (8), 1155–1173.

Ishai, O., Bodner, R., 1970. Limits of linear viscoelasticity and yield of a filled and unfilled epoxy resin. Transactions of the Society of Rheology 14 (2), 253–273.

Ismael, N.F., Mollah, M.A., 1998. Leaching effects on properties of cemented sands in Kuwait. Journal of Geotechnical and Geoenvironmental Engineering 124 (10), 997–1004.

Lemarchand, E., Ulm, F.-J., Dormieux, L., 2002. The effect of inclusions on the friction coefficient of highly filled composite materials. Journal of Engineering Mechanics ASCE 128 (8), 876–884.

Li, G.Q., Zhao, Y., Pang, S.S., 1999. Four-phase Sphere modeling of effective bulk modulus of concrete. Cement and Concrete Research 29 (6), 839–845.

Lutz, M.P., Zimmerman, R.W., 1996. Effect of the interphase zone on the bulk modulus of a particulate composite. Journal of Applied Mechanics—Transactions of the ASME 63 (4), 855–861.

Lutz, M.P., Monteiro, P.J.M., Zimmerman, R.W., 1997. Inhomogeneous interfacial transition zone model for the bulk modulus of mortar. Cement and Concrete Research 27 (7), 1113–1122.

Maso, J.C., 1996. Interfacial Transition Zone in Concrete. Report 11. RILEM.

Mehta, P.K., Monteiro, P.J.M., 1988. Effect of aggregate, cement, and mineral admixtures on the microstructure of the transition zone. In: Mindess, S., Shah, S.P. (Eds.), Proceedings of Symposium on Bonding in Cementitious Materials, vol. 114. Materials Research Society.

Monteiro, P.J.M., Ostertag, C.P., 1989. Analysis of the aggregate cement paste interface using grazing-incidence X-ray scattering. Cement and Concrete Research 19 (6), 987–988.

Ponte Castaneda, P., 1991. The effective mechanical properties of nonlinear isotropic composites. Journal of Mechanics and Physics Solids 39, 45–71.

Ramesh, G., Sotelino, E.D., Chen, W.F., 1996. Effect of transition zone on elastic moduli of concrete materials. Cement and Concrete Research 26 (4), 611–622.

Re, G.Da., 2000. Physical mechanisms controlling the pre-failure stress–strain behavior of frozen sand. PhD Dissertation, MIT.

Suquet, P., 1997. Effective Properties of Nonlinear Composites. In: Continuum Micromechanics. In: Suquet, P. (Ed.), CISM Courses and Lectures, no. 377. Springer, New York, pp. 197–264.

Suresh, S., Mortensen, A., 1998. Fundamentals of Functionally Graded Materials: Processing and Thermomechanical Behaviour of Graded Metals and Metal–Ceramic Composites. Cambridge University Press, Cambridge, UK.

Ulm, F.-J., Heukamp, F.H., Germaine, J.T., 2002. Residual design strength of cement-based materials for nuclear waste storage systems. Nuclear Engineering and Design, 51–60.

Yuji, W., 1988. The effect of bond characteristics between steel slag fine aggregate and cement paste on mechanical properties of concrete and mortar. In: Mehta and Monteiro (1988).

Zaoui, A., 2002. Continuum micromechanics—a survey. Journal of Engineering Mechanics ASCE 128 (8), 808–816.